Surface Hydration Drives Rapid Water Imbibition into Strongly Hydrophilic Nanopores

Chao Fang and Rui Qiao*

Department of Mechanical Engineering, Virginia Tech, Blacksburg, VA 24061

ABSCTRACT:

The imbibition of liquids into nanopores plays a critical role in numerous applications, and most prior studies focused on imbibition due to capillary flows. Here we report molecular simulations of the imbibition of water into single mica nanopores filled with pressurized gas. We show that, while capillary flow is suppressed by the high gas pressure, water is imbibed into the nanopore through surface hydration in the form of monolayer liquid films. As the imbibition front moves, the water film behind it gradually densifies. Interestingly, the propagation of the imbibition front follows a simple diffusive scaling law. The effective diffusion coefficient of the imbibition front, however, is more than ten times larger than the diffusion coefficient of the water molecules in the water film adsorbed on the pore walls. We clarify the mechanism for the rapid water imbibition observed here.

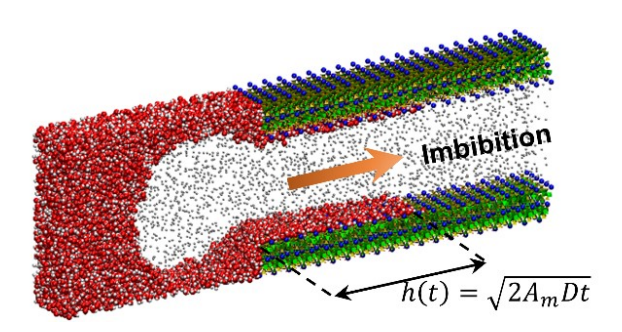


Table of contents entry: Surface hydration-driven imbibition of water into strongly hydrophilic pores observes a diffusive scaling law and exhibits effective diffusion coefficients much higher than water molecules.

^{*} To whom correspondence should be addressed. Email: ruiqiao@vt.edu.

1. Introduction

Imbibition and infiltration of liquids into nanopores play a critical role in diverse applications including lab-on-chip, oil and gas recovery, smart textiles, and energy storage. ¹⁻⁴ In recent years, driven by the advancement in nanochannel fabrication and computational methods, ⁵ there has been a surge of interest in understanding these phenomena beyond the classical interpretation pioneered by Lucas and Washburn a century ago. Indeed, research on these phenomena has evolved into one of the most exciting frontiers in the nanofluidics field, with new phenomena discovered and new fundamental insights offered. For example, even though the classical Washburn law, in which the movement of the imbibition front exhibits a square root law scaling, has been confirmed in smooth nanopores, ⁶ qualitative and quantitative deviations from this law have also been identified. ⁷⁻¹² In particular, slippage at liquid-wall interfaces, ^{9, 13, 14} disjoining pressure in liquid films, ^{13, 15} electroviscous effects, ^{7, 16} enhanced viscosity of interfacial or highly confined fluids, ¹⁷ and contact angle hysteresis ¹⁸ have been shown to greatly affect liquid imbibition into nanopores.

Most of the existing studies focused on imbibition associated with capillary flows. However, imbibition can also occur via other mechanisms. In particular, surface hydration, the imbibition of water into nanopores driven by the affinity of water molecules to strongly hydrophilic pore walls, can lead to water imbibition without involving capillary flow. Despite the potential relevance of surface hydration in technically important problems such as water management in shale gas recovery operations, ^{20, 21} a fundamental understanding of such imbibition is limited at present.

In this work, we investigate the imbibition of water into slit mica nanopores filled with highly pressurized methane using molecular dynamics (MD) simulations. Since the capillary pressure is smaller than the initial gas pressure inside the pore, imbibition through capillary flow is suppressed. Nevertheless, water is imbibed into the pore through surface hydration in the form of a monolayer liquid film before the imbibition front reaches the pore's end. We show that the growth of the imbibition front driven by surface hydration follows a simple diffusive scaling law. Interestingly, the effective diffusion coefficient for the growth of the imbibition front is more than an order of

magnitude larger than the self-diffusion coefficient of the water molecules in the thin water film adsorbed on pore walls. With the help of a molecular theory, we clarify the mechanism underlying the rapid water imbibition observed during surface hydration.

2. Simulation System and Methods

System and simulation protocol. Figure 1 shows a schematic of the MD system for studying the imbibition of water into a slit-shaped nanopore. The system consists of a water reservoir and a slit pore cleaved from mica, which is a good model for strongly hydrophilic materials. The pore is 6nm wide, 3.15nm deep in the y-direction, and 20.2nm long in the x-direction. The right end of the pore is sealed. The system is periodical in all three directions. To reduce the effects of periodicity on water imbibition, the simulation box is 36.5nm long in the pore length direction. Initially, the pore is separated from the water reservoir by "blocker" atoms at its entrance (the red dots in Fig. 1) and is filled with methane at 250bar. The pressure of the water reservoir is controlled using a piston to 5bar. The MD system is first equilibrated for 1ns. Next, the blocker atoms are removed to initiate water imbibition (this time instant is defined as t=0), and the system is run for 8ns to study the water imbibition. We note that the imbibition of fluids into the pore is not driven by the

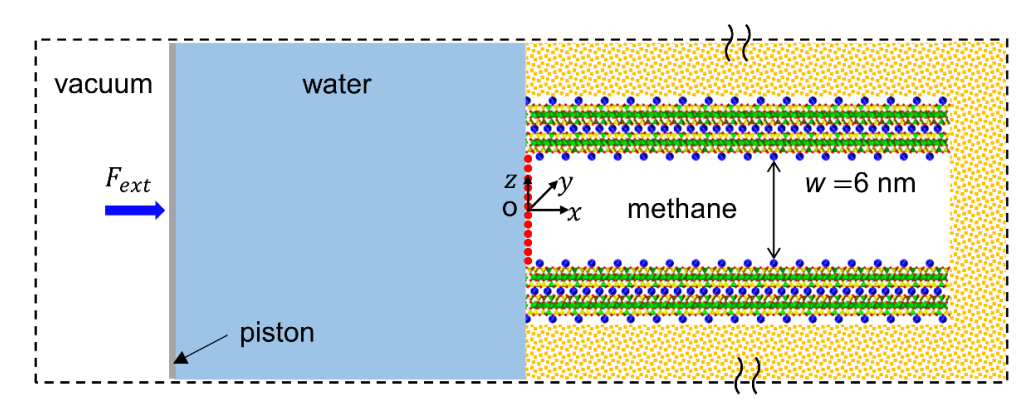


Figure 1. A schematic of the system for studying water imbibition into slit mica pores. The pore is initially separated from the water reservoir by blocker atoms (red dots) and filled with methane. The pressure in the reservoir is controlled using a piston. Implicit walls (denoted by the golden slabs) are used to model the mica away from the imbibed water. The dashed lines denote the periodical simulation box. At t = 0, the blocker atoms are removed to initiate water imbibition. x=0 corresponds to the pore entrance. The Figure is not drawn to scale. A 3D view of the system is shown in the Electronic supplementary information.

pressure applied on the piston. Indeed, we found that different applied pressure (e.g., 10bar) on the piston does not notably affect the water imbibition as long as capillary flow into pore is suppressed.

Molecular model. To reduce computational cost, only the horizontal pore walls that can come into contact with the imbibed water molecules are modeled atomistically. The other portion of the pore walls that do not directly affect the water imbibition are modeled as implicit walls (see below). Each of the atomistic walls is made of two muscovite mica layers (~2nm thick) so that the water-wall interactions are captured accurately. Muscovite (KAl₂Si₃AlO₁₀(OH)₂) is a phyllosilicate clay.²² Each muscovite layer has a tetrahedral-octahedral-tetrahedral (TOT) structure, in which each Al-centered octahedral sheet is sandwiched between two Si-centered tetrahedral sheets. The neighboring TOT structures are held together by a potassium interlayer. Following the widely used method for building surfaces and nanopores from muscovite minerals, we cleave the muscovite such that its surface features K⁺ ions and is rich in bridging oxygen atoms.^{22, 23}

Water and methane are modeled using the SPC/E model and the TraPPE force fields.²⁴ The partial charges and LJ parameters for the mica atoms are taken from the CLAYFF force fields.^{22, 25} The TraPPE force fields enables accurate prediction of methane's thermodynamic properties. In addition, prior works showed that the CLAYFF force fields allow the surface hydration of clay surfaces under equilibrium conditions to be accurately simulated.^{23, 26} The interactions among mica atoms are excluded. Atoms in the clay sheets in contact with methane or water are tethered with a stiff spring to their lattice sites. Other atoms in the mica walls are fixed. For the portion of the mica wall modeled implicitly, their interactions with the methane molecules and the oxygen atoms of water molecules are computed using the LJ 12-6 potential

$$E(s) = 4\epsilon \left[\left(\frac{\sigma}{s} \right)^{12} - \left(\frac{\sigma}{s} \right)^{6} \right] \tag{1}$$

where s is the separation between a methane molecule (or the oxygen atom of a water molecule) and the surface of the *nearest* implicit wall. To mimic strongly hydrophilic walls, σ =0.287nm and ϵ =6.23kJ/mol are adopted for the water-wall and the methane-wall interactions.

All simulations are carried out using the LAMMPS code²⁷ in the NVT ensemble (T=300K).

The equations of motion are solved using a time step of 1fs. The vibrating mica atoms are kept at a constant temperature using a Nose-Hoover thermostat. Bond lengths and angles of the water molecules are kept fixed using the SHAKE algorithm. The temperature of the water and methane molecules are maintained using the dissipative particle dynamics (DPD) thermostat which has the advantage of preserving hydrodynamics. ¹⁴ Non-electrostatic forces are computed using the cutoff method (cutoff length: 1.2nm). Long-range electrostatic forces are computed using the particle-particle particle-mesh (PPPM) method²⁸ with a relative accuracy of 10⁻⁵.

3. Results and Discussion

Imbibition dynamics. Figure 2a shows that, after the blocker atoms at the pore entrance are removed, the methane gas expands into the water reservoir to form a bubble at the pore entrance, and its size remains relatively unchanged during the simulation. The flow of water across the full pore width is not observed. Instead, water enters the pore as two thin liquid films and the length of these thin films grows with time. In principle, the film growth can occur by two processes. First, the water molecules in the film can propagate along the pore's two walls and thus the liquid film extends deeper into the pore with time. Second, water molecules in the meniscus and/or liquid film can enter the gas phase, transport into the pore interior and subsequently adsorb on the pore wall.²⁹ We carefully examined the simulation trajectory and find that the second process contributes negligibly to the growth of the liquid film in the system studied here. We envision that this second process may become important in wide pores and at higher temperature because both evaporation and transport of water molecules are facilitated in these situations.

Since the liquid film growing laterally on the pore wall is about one molecule thick (see below) and thus the concept of hydrodynamic flow is not readily applicable, the water imbibition observed here is best regarded as surface hydration. Importantly, the imbibition observed here is truly a surface phenomenon and its dynamics does not depend on the pore width. The idea is corroborated by two observations. First, the thickness of the water film on the pore walls is <1nm, which is much smaller the pore width. Hence, the water film on one pore wall does not "see" the other pore

wall. It follows that the effect of one pore wall on the growth of water film on the other pore wall is negligible – as far as the film growth is concerned, the pore width is not important here. Second, the thin liquid film propagating into the pore resembles the thin precursor films ahead of liquids imbibed into a pore by capillary flow or a spreading droplet, 6, 30-32 whose occurrence does not depend on the width/length of pore or the size of the droplet either. As we shall see later, the growth of the imbibed water film in the present simulations follows the same scaling law for those precursor films. As long as the imbibition front does not reach the pore's dead end, the pore length has no impact on the imbibition dynamics either. Therefore, although water imbibition is simulated in a relatively narrow and short pore, the insight gained here is also relevant to imbibition into wider and longer pores.

To quantify the dynamics of imbibition, we compute the evolution of the number of water molecules imbibed into the pore N(t) and the propagation of the imbibition front h(t) along the pore walls. To determine h(t), we first compute the area density of water molecules on the pore walls as a function of distance from the pore entrance, $\rho_s(x,t)$, by taking advantage of the

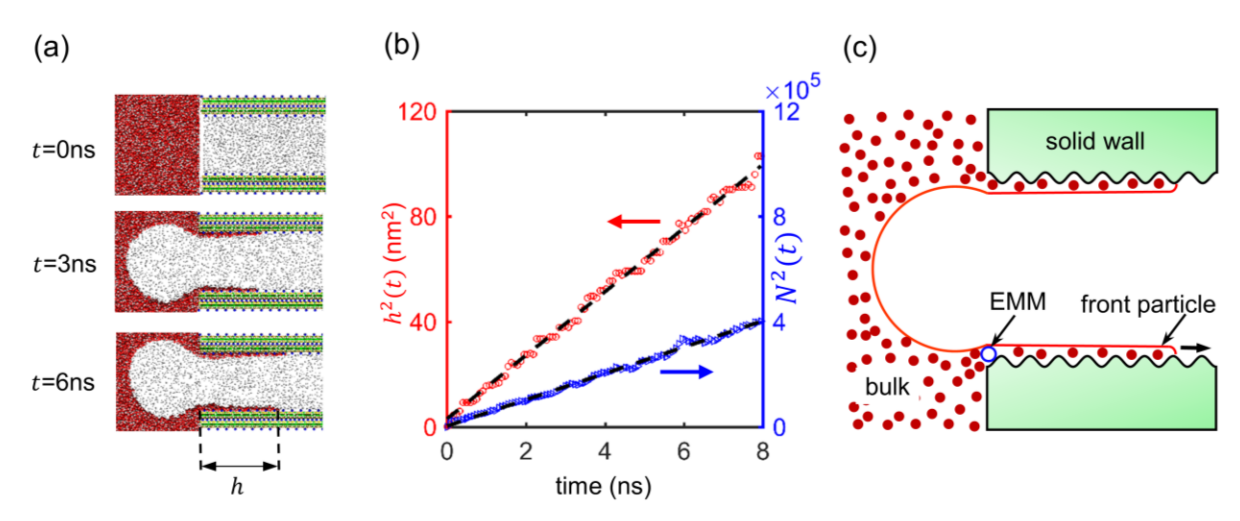


Figure 2. Dynamics of imbibition driven by surface hydration. (a) Snapshots of the system near the pore entrance during imbibition. Water is imbibed into the pore as thin films on the pore walls. (b) Evolution of the imbibition front $h^2(t)$ and the number of water molecules imbibed into the pore $N^2(t)$ as a function of time. The imbibition exhibits a diffusive scaling law since $h^2(t)$ and $N^2(t)$ increase linearly with time. (c) A schematic of the molecular model for the propagation of thin liquid films on wetting solid substrates developed by Burlatsky, Oshanin, Cazabat and Moreau. This panel is adapted from Ref. 33.

fact that the imbibed water molecules form a thin film on the pore walls. Next, we scan $\rho_s(x,t)$ from pore interior toward the pore entrance, and the imbibition front h(t) is marked as the position at which $\rho_s(x,t)$ exceeds a threshold value of $\rho_s^{th}=0.4$ nm⁻². Figure 2b shows that $h^2(t)$ increases linearly with time, i.e., the movement of the imbibition front follows a diffusive scaling law $h(t) \sim t^{1/2}$. Using a diffusive growth law $h(t) = \sqrt{2D_e t}$ and the data in Fig. 2b, the effective diffusion coefficient D_e of the growth of the imbibed water film's length is found to be 6.02×10^{-9} m²/s. Figure 2b shows that the growth of the amount of imbibed water molecules also follows a diffusive scaling law, i.e. $N^2(t) \sim t$ or $N(t) \sim t^{1/2}$. Together, these results show that the imbibition of water into a nanopore by surface hydration is a dynamic process observing a diffusive scaling law. It is useful to note that such a scaling law is also observed for the spreading of precursor films ahead of liquids imbibed into a pore via capillary flow or a spreading droplet. 6, 32

To further delineate the imbibition process, we quantify the temporal and spatial distribution of hydration water layer propagating on the pore walls. Figure 3a shows the evolution of the average water density profiles normal to the lower mica wall in two selected patches along the pore (patch A: x=1.5-2.5nm; Patch C: x=3.5-4.5nm). We observe that the imbibed water forms a single layer on the pore walls. After the imbibition front moves past a patch on the pore walls, the thickness of the water layer in that patch does not increase but the amount of water adsorbed there can still increases. For example, at t=1ns, the imbibition front already reaches the surface patch C located at x=3.5-4.5nm, but more water molecules become adsorbed on the surface patch A located at x=1.5-2.5nm till $t\sim7$ ns. Similar trend is evident in Fig. 3b, which shows the temporal evolution of the area density of water molecules in several patches on the pore wall. These results imply that, although surface hydration-driven imbibition involves the propagation of a monolayer water film along the pore, the density of the water film is not a constant. In fact, the water monolayer behind the imbibition front densifies as the imbibition front moves forward. To see this from a different perspective, we compute the area density of the water molecules adsorbed on the pore wall, $\rho_s(x, y, t)$, at a representative time of t=6.5ns, when the imbibition front has reached x = 9.0nm. Figure 3c shows $\rho_s(x, y, t)$ near the imbibition front. While the surface sites in the region 8 nm < x < 8.6 nm are occupied by many water molecules, the interstitial spaces between the surface K^+ ions behind the imbibition front are only sparsely populated by water molecules. As one moves from the imbibition front toward the pore entrance, the interstitial spaces between the surface K^+ ions become more densely populated by water molecules. Together, the results in Fig. 3b and 3c show that, as the imbibition front moves forward, the most favorable surface sites near the imbibition front are hydrated by water molecules first and the less favorable surface sites behind the imbibition front gradually become hydrated by water molecules. Consequently, while the thickness of the water film is nearly uniform over the pore walls, the density of the water film decreases as one moves from the pore entrance toward the imbibition front.

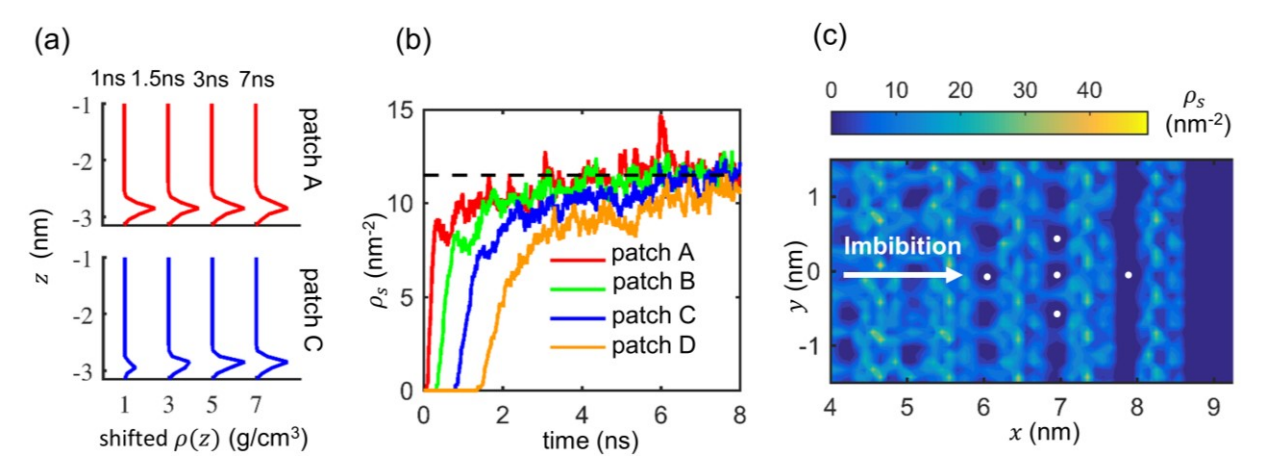


Figure 3. Temporal evolution and spatial distribution of hydration water on pore walls during imbibition. (a) Evolution of the water density profile normal to the lower mica wall in two surface patches of the wall (patch A: x=1.5-2.5nm; patch C: x=3.5-4.5nm; x=0 corresponds to the pore entrance). The water density profiles at t=1, 1.5, 3, and 7ns are *shifted up* by 1, 3, 5, and 7g/cm³ for clarity. z=-3nm corresponds to the position of the surface K^+ ions on the lower mica wall. (b) Growth of the area density of hydration water in different patches along the mica wall (patch A: x=1.5-2.5nm; patch B: x=2.5-3.5nm; patch C: x=3.5-4.5nm; patch D: x=4.5-5.5nm). The dashed line denotes the asymptotic area density of water on the wall. (c) The distribution of water density on a portion of the pore walls at t=6.5ns. Some of the K^+ ions on the mica surface are identified using white dots. The position of water molecules is determined based on their oxygen atom.

Molecular model of surface hydration. The essential features of the imbibition dynamics revealed in Fig. 2 and 3 can be captured by the thin film growth theory developed by Burlatsky,

Oshanin, Cazabat, and Moreau two decades ago.³³ This theory considers the growth of a single molecule-thick liquid film originating from a stationary liquid meniscus (see Fig. 2c). It was postulated that the growth of a molecularly thin film is governed by the diffusive transport of vacancies from its front to the edge of the macroscopic meniscus (EMM). The analytical model building on this idea predicts that the liquid density (molecular vacancy) in the thin film increases (decreases) as the one moves from the tip of the propagating film toward the EMM, which is observed in our simulations. Moreover, in agreement with the imbibition characteristics shown in Fig. 2b and c, solution of the analytical model indicates that the growth of the liquid film follows a diffusive scaling law, i.e., the growth of the total mass of the liquid film and the movement of the liquid film's front both follow a square root law. For example, the front of the liquid film h(t) moves along the solid substrate by

$$h(t) = \sqrt{2A_m Dt} \tag{2}$$

where D is the diffusion coefficient of liquid molecules in the thin film. On homogeneous solid substrates, A_m is a constant controlled by two energies: the energy gained by moving a liquid molecule from the interior of the macroscopic meniscus into a vacancy site at EMM (E_{\downarrow}) and the work needed for moving a vacancy at the tip of a laterally propagating liquid film (W_{\leftarrow}) to the EMM (see Fig. 2c). It follows that the propagation of the liquid film's tip exhibits an effective diffusion coefficient of $A_m D$, and this effective diffusion coefficient is affected by the liquid-substrate interactions at the EMM and at the front of liquid film. A key prediction of the theory, which has not been examined thus far to our best knowledge, is that A_m can be either smaller or larger than one depending on the value of E_{\downarrow} and W_{\leftarrow} . Si Given that the theory captures the qualitative aspect of surface hydration well, we next investigate quantitatively how large A_m is in the present system, and in particular, whether A_m may be larger than one. To this end, we first examine the diffusion of water molecules in monolayer water films adsorbed on mica surfaces.

Dynamics of water molecules in thin films. We perform *separate* equilibrium simulations in which a layer of water molecules is placed on the mica walls (see Electronic Supplementary Information (ESI)). The area density of water molecules is set to the asymptotic water density on

the mica surface at positions far behind the imbibition front observed in Fig. 3b. Figure 4a shows the mean square displacements (MSDs) of the water molecules in x- and y- directions, which give diffusion coefficients of D_x =0.42×10⁻⁹ m²/s and D_y =0.6×10⁻⁹m²/s in the x- and y- directions, respectively. Both D_x and D_y are much smaller than that of bulk water (D_{bulk} =2.54×10⁻⁹m²/s), in good agreement with prior reports.

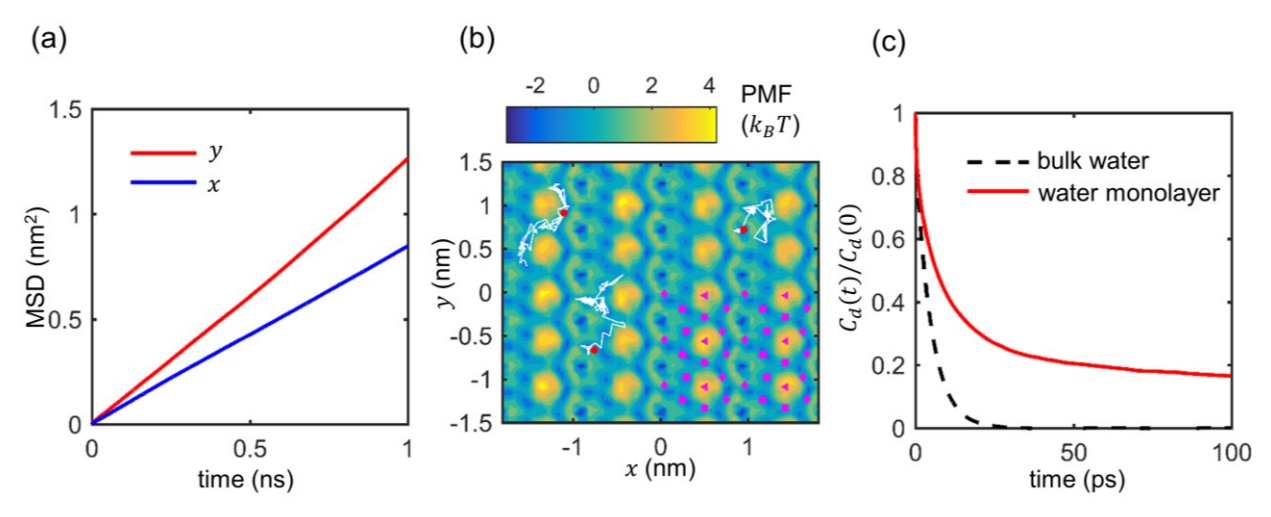


Figure 4. Dynamics of water molecules in the water monolayer adsorbed on planar mica surfaces. (a) The mean square displacement (MSD) of water molecules in x- and y- directions. (b) The trajectory of three representative water molecules over 200ps. The red dots denote the initial position of the water molecules. The trajectory is overlaid on the color-coded PMF plot of the water molecules on the mica surface. The magenta markers in the right bottom corner denote some of mica's surface atoms (K⁺ ions: triangle; bridging oxygen: square; bridging oxygen with tetrahedral substitution: diamond). (c) The dipole autocorrelation function (dashed line is for water molecules in bulk) of water molecules.

To understand the slow diffusion of water molecules adsorbed on the mica surface and its anisotropicity, we compute the potential of mean force (PMF) of water molecules adsorbed on the mica wall (see ESI). Figure 4b shows that the free energy landscape for water molecules diffusing over the mica wall is highly corrugated. Because of the strong hydrogen-bonding between water molecules and the bridging oxygen atoms on the mica surface and between water molecules and the surface K^+ ions (see Fig. 4b), there are distinct free energy valleys near the bridging oxygen atoms and surface K^+ ions. Meanwhile, the protrusion of surface K^+ ions from the mica wall creates free energy hills above the K^+ ions and saddle points between vertically aligned K^+ ions (see Fig.

4b). When performing random walks over such a corrugated energy landscape, water molecules are often trapped into local energy minimums (see trajectories of representative water molecules in Fig. 4b), hence exhibiting slow diffusion. The anisotropicity of water diffusion in the *x*- and *y*-directions originates from the anisotropicity of the PMF: because the free energy landscape is more corrugated in the *x*-direction (see Fig. 4b), the diffusion in *x*-direction is slower.

In addition, because of the strong, directional interactions between water molecules and the bridging oxygen atoms and surface K^+ ions on the mica walls, water molecules often adopt preferred orientation with respect to these atoms, which hinders their free rotation. This is evident from the dipole autocorrelation function $C_d(t)$ of water molecules shown in Fig. 4c. For water molecules in the bulk, $C_d(t)$ decays to zero in ~20ps. However, for water molecules adsorbed on the mica surface, their $C_d(t)$ reaches only ~0.3 by 20ps, and decays very lowly after that. Since the translation of water molecules over the heterogeneous surface of a mica wall inevitably requires them to rotate from time to time, the retardation of the rotation of water molecules hinders their translational diffusion.

Accelerated diffusion of the imbibition front. We now return to the dynamics of imbibition driven by surface hydration. Using the effective diffusion coefficient for the growth of imbibition front and the D_x of the water molecules computed above, it follows from Equ. 2 that $A_m \sim 14$, i.e., the growth of the imbibition front is greatly accelerated compared to the diffusion of individual water molecules in single-molecule thick hydration layer. This thus supports the prediction of Burlatsky *et al.*'s theory that A_m can be larger than 1. Based on their theory, this large A_m indicates that $E_{\downarrow} \gg k_B T$ and $W_{\leftarrow} \ll k_B T$ ($k_B T$ is the thermal energy) in our system. E_{\downarrow} is the energy gain when a water molecule is moved from bulk to fill a vacancy at the EMM. Hence $E_{\downarrow} \gg k_B T$ corresponds to strong liquid-substrate attractions. W_{\leftarrow} is the cost of moving a vacancy from the tip of the imbibed film to the EMM. In the theory by Burlatsky *et al.*, this cost is equivalent to the difference of the energies lost and gained due to the forward (i.e., moving away from the EMM) and backward hop of the front molecule of the imbibed film. ³³ Computing E_{\downarrow} and W_{\leftarrow} is difficult because, unlike in the theory where molecules are assumed to occupy defined lattices, water

molecules are randomly distributed on the mica wall in our simulations and thus vacancies are not well-defined. Nevertheless, we can gain insight into E_{\downarrow} and W_{\leftarrow} by examining the energetics of water molecules in mica-water systems and thus better understand the accelerated diffusion of the imbibition front.

To gain insight into E_{\downarrow} , we note that the liquid structure at EMM is intermediate between that of the water at the interface of a thick water layer and a mica surface and that of a monolayer water film adsorbed on a mica wall. Therefore we compute the potential energy of a water molecule when it is located at three positions: in bulk water (E_1) , in the first interfacial water layer near mica wall hydrated by a thick slab of water (E_2) , and in a monolayer water film adsorbed on a mica wall $(E_3$, the water density here is equal to the asymptotic water density in the imbibed water film shown in Fig. 3b). Snapshots of the water molecules at these positions and their microenvironments are shown in Fig. S2 in the ESI. A value of -18.65, -21.38, -19.58 k_BT is obtained for E_1 , E_2 , and E_3 , respectively. In particular, E_2 and E_3 are 2.73 and 0.93 k_BT smaller than E_1 , respectively. This indicates that when a water molecule moves from bulk to the EMM, the increase of its potential energy due to the reduction of its number of neighboring water molecules is compensated by its strong attraction by the mica wall. This strong attraction of water by the mica wall is consistent with the strong electrostatic interactions between the water molecule and the charged sites on the mica wall. To qualitatively understand W_{\leftarrow} , we next compute the potential energy of an isolated water molecules adsorbed on the mica wall (E_4) , and find it to be lower than E_3 by $3.00k_BT$. Therefore, it is energetically favorable for a water molecule at the imbibition front to hop forward. Specifically, when a water molecule at the imbibition front hops forward, its potential energy tends to increase because it loses the coordination by neighboring water molecules. However, at the same time, this water molecule improves its coordination with the charged sites on the mica surface (see Fig. S3 in the ESI), and thus its potential energy due to interactions with the mica surface becomes more negative. The latter effect is more significant and hence forward hopping is energetically favorable. While the net free energy cost for a water molecule at the imbibition front to hop forward can still be positive because isolated water molecules are confined tightly to selected surface sites and thus suffer an entropy penalty, the forward hoping should be a facile process and hence W_{\leftarrow} is small. Overall, the above results show that the accelerated diffusion of the imbibition front compared to the diffusion of individual water molecules in thin water films adsorbed on mica walls (i.e., $A_m > 1$) is caused by the strong attraction of water molecule by the mica walls. In the present study, the pore walls are homogeneous in both physical structure and chemical nature, and thus A_m is a constant. For pore walls with heterogeneous surface properties, A_m may not be a constant.

4. Conclusions

In summary, we studied the imbibition of water into mica nanopores filled with pressurized methane gas using molecular dynamic simulations. While capillary flow through the pore's full cross-section is suppressed, water invades the pore as monolayer water films propagating on the pore walls. The growth of the imbibition front during this surface hydration-dominated process follows a diffusive scaling law. The effective diffusion coefficient of the growth of the imbibition front is more than one order of magnitude larger than that of individual water molecules in the water film, which is attributed to the fact that the interactions between water molecules and mica walls are stronger than that between water molecules in the water film and in bulk.

In the present study, we considered only the imbibition of water into mica pores through surface hydration. The scaling law revealed here should be applicable to the imbibition of fluids as thin liquid films when other imbibition modes (e.g., capillary flow) is suppressed. However, for such imbibition to occur, the fluid molecules must show strong affinity to the solid surface (e.g., if the fluids shows complete wetting on the surface). This condition is similar to that for the formation of a precursor film ahead of a spreading droplet or the liquids imbibed into a pore by capillary flow, and it is embodied in the requirement that the term E_{\downarrow} in Burlatsky *et al*'s model must be large. If the pore walls are made of materials much less hydrophilic than mica, this condition may not be met and thus water transport through surface hydration may not occur.

References

- 1. L. Liu, X. Chen, W. Lu, A. Han and Y. Qiao, *Phys. Rev. Lett.*, 2009, 102, 184501.
- 2. N. R. Tas, J. Haneveld, H. V. Jansen, M. Elwenspoek and A. van den Berg, *Appl. Phys. Lett.*, 2004, 85, 3274-3276.
- 3. S. Gruener, T. Hofmann, D. Wallacher, A. V. Kityk and P. Huber, *Phys. Rev. E*, 2009, 79.
- 4. R. B. Schoch, J. Han and P. Renaud, Rev. Mod. Phys., 2008, 80, 839-883.
- 5. C. Duan, W. Wang and Q. Xie, Biomicrofluidics, 2013, 7, 026501.
- 6. D. I. Dimitrov, A. Milchev and K. Binder, *Phys. Rev. Lett.*, 2007, 99.
- 7. S. Das and S. K. Mitra, *Phys. Rev. E*, 2013, 87.
- 8. G. Cao, Y. Qiao, Q. Zhou and X. Chen, *Philos. Mag. Lett.*, 2008, 88, 371-378.
- 9. S. Supple and N. Quirke, *Phys. Rev. Lett.*, 2003, 90.
- 10. K. Yamashita and H. Daiguji, *J. Phys. Chem. C*, 2015, 119, 3012-3023.
- 11. J. Mo, L. Li, J. Zhou, D. Xu, B. Huang and Z. Li, *Phys. Rev. E*, 2015, 91, 033022.
- E. Oyarzua, J. H. Walther, A. Mejia and H. A. Zambrano, *Phys. Chem. Chem. Phys.*, 2015, 17, 14731-14739.
- 13. B. Henrich, C. Cupelli, M. Santer and M. Moseler, New J. Phys., 2008, 10.
- 14. L. Joly, J. Chem. Phys., 2011, 135, 214705.
- 15. S. Gravelle, C. Ybert, L. Bocquet and L. Joly, *Phys. Rev. E*, 2016, 93.
- 16. N. Desai, U. Ghosh and S. Chakraborty, *Phys. Rev. E*, 2014, 89.
- 17. T. Q. Vo, M. Barisik and B. Kim, *Phys. Rev. E*, 2015, 92.
- 18. C. Bakli and S. Chakraborty, Appl. Phys. Lett., 2012, 101.
- 19. J. K. Mitchell, Fundamentals of Soil Behavior, John Wiley, London, 1993.
- 20. R. W. Howarth, A. Ingraffea and T. Engelder, *Nature*, 2011, 477, 271-275.
- 21. H. Singh, J Nat Gas Sci Eng, 2016, 34, 751-766.
- 22. T. A. Ho and A. Striolo, *AIChE J.*, 2015, 61, 2993-2999.
- 23. A. Malani and K. G. Ayappa, *J. Phys. Chem. B*, 2009, 113, 1058-1067.
- 24. M. G. Martin and J. I. Siepmann, *J. Phys. Chem. B*, 1998, 102, 2569-2577.

- 25. R. T. Cygan, J.-J. Liang and A. G. Kalinichev, J. Phys. Chem. B, 2004, 108, 1255-1266.
- 26. D. Argyris, D. R. Cole and A. Striolo, *ACS Nano*, 2010, 4, 2035-2042.
- 27. S. Plimpton, J. Comput. Phys., 1995, 117, 1-19.
- 28. R. W. Hockney and J. W. Eastwood, *Computer simulation using particles*, CRC Press, 1988.
- 29. P. Huber, J. Phys. Condens. Matter, 2015, 27, 103102.
- 30. S. Chibbaro, L. Biferale, F. Diotallevi, S. Succi, K. Binder, D. Dimitrov, A. Milchev, S. Girardo and D. Pisignano, *Europhys. Lett.*, 2008, 84, 44003.
- 31. M. Khaneft, B. Stühn, J. Engstler, H. Tempel, J. J. Schneider, T. Pirzer and T. Hugel, *J. Appl. Phys.*, 2013, 113, 074305.
- 32. M. N. Popescu, G. Oshanin, S. Dietrich and A. Cazabat, *J. Phys. Condens. Matter*, 2012, 24, 243102.
- 33. S. F. Burlatsky, G. Oshanin, A. M. Cazabat and M. Moreau, *Phys. Rev. Lett.*, 1996, 76, 86-89.
- 34. V. Marry, E. Dubois, N. Malikova, J. Breu and W. Haussler, *J. Phys. Chem. C*, 2013, 117, 15106-15115.
- 35. C. P. Morrow, A. Ö. Yazaydin, M. Krishnan, G. M. Bowers, A. G. Kalinichev and R. J. Kirkpatrick, *J. Phys. Chem. C*, 2013, 117, 5172-5187.
- 36. B. F. Ngouana W and A. G. Kalinichev, *J. Phys. Chem. C*, 2014, 118, 12758-12773.